Finite Element Study on 1-D Array Transducer Design

Wenkang Qi and Wenwu Cao

Abstract—**A comprehensive study using finite element analysis (FEA) was performed on 1-D transducer arrays. Crosstalk reduction, subdicing effects, directivity pattern, and baffle effects were quantified numerically. It was found that the directivity pattern strongly depends on the transducer size and kerf filling materials. The FEA is particularly powerful to reveal the inhomogeneous nature of the vibrational characteristic of transducer surface, which allows more accurate beam pattern computation in 3-D. The simulated directivity pattern also was satisfactorily verified by experimental measurements.**

I. Introduction

Ultrasonic transducer arrays are widely used in clinical ultrasound diagnosis [1]. Designing better array transducers is the critical issue for further improving the quality of ultrasonic imaging. For this purpose, it is necessary to gain better fundamental understanding on the transducer operations in order to design new and better arrays. Many issues in array design—such as crosstalk, baffle effect, directivity pattern—cannot be accurately studied using analytic method due to the complexity of the partial differential equations involved. Finite element analysis (FEA) is the only appropriate way to gain more detailed information [2].

Reducing the element crosstalk level is very important in array designs, especially for phased arrays, because the crosstalk between elements affects the directivity pattern and the sensitivity. Another important issue in transducer design is to avoid lateral modes, which may couple to the thickness mode to affect the transducer operation, similar to the case of single-element composite transducers [3]–[9]. Subdicing of the elements has been used in practice to solve this lateral mode problem. It also was shown experimentally that using lossy kerf filler material could substantially reduce those lateral modes. Here we will use simulation to help understand the mechanism of these practical methods employed by many transducer engineers.

Under 1-D approximation, the baffle effects on an array element can be described by a $\cos\theta$ function as described in most of the existing literature, which implies that the baffle was treated as a pressure-release baffle and the array was assumed to be infinite in size. Using FEA, we can show that the baffle effect is much more complicated than a $\cos\theta$ function because the actual array is always finite in size, and the baffle is not purely the pressure-release type. This paper will provide more technical details for the 1-D array design through FEA simulations.

Most of the results were obtained using the ANSYS finite element package, and the general meshing scheme is to maintain at least 8 elements per wavelength. Optimized meshing size was obtained by continuously reducing the element size until the relative error for a calculated target quantity between consecutive runs is less than 1%. Because very large simulation models become numerically unstable, we used the boundary element method (BEM) for transducer beam pattern calculation and obtained satisfactory results.

Manuscript received July 28, 1999; accepted February 3, 2000. This research is supported by the national resource grant from the NIH Grant # p41-RR11795-01A1.

W. Qi currently is with GE Diasonics, San Jose, CA 95112.

W. Cao is with the Materials Research Laboratory, The Pennsylvania State University, University Park, PA 16802 (e-mail: cao@math.psu.edu).

II. Effects of Subdicing, Baffle Influence and Directivity Pattern

A. Effect of Subdicing

As a requirement, the width, d, of each element in a 1-D array should be large enough so the acoustic impedance loaded on the element will not be purely imaginary (in which case the element cannot radiate acoustic energy into the medium). However, the aspect ratio h/d of each element must be greater than 2 in order to separate the lateral modes from the thickness mode, where h is the height of the element.

In many current 1-D array transducers, each element is subdiced, which can effectively decrease the aspect ratio of each element. Our simulation results demonstrated the importance of element subdicing. Fig. 1 shows the impedance spectrum for a 1-D array with the kerf width, element size, and element height to be 50 μm, 200 μm, and 300 μm, respectively. This design does not obey the rule of aspect ratio > 2; therefore, one can clearly see a lateral mode on the impedance curve near 7 MHz (see the solid line). When all the elements in the array are subdiced to make the aspect ratio greater than 2, the lateral mode disappeared as shown in the dashed line in Fig. 1. The lateral mode was not suppressed by the subdicing; it was simply being pushed to frequencies much higher than the thickness mode.

Introducing high mechanical damping into the filler material also can reduce the amplitude of the lateral modes in 1-D arrays, particularly in high frequencies. Fig. 2 shows

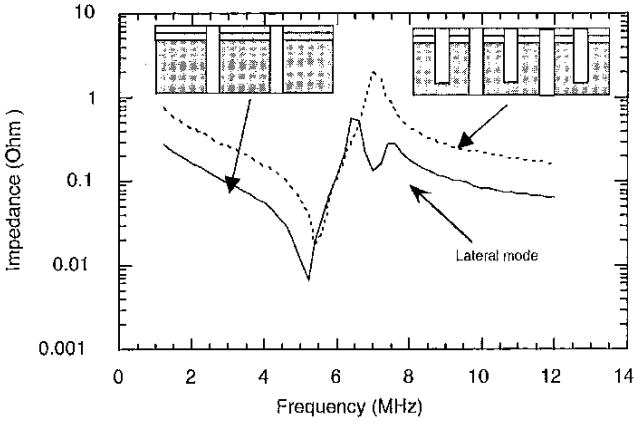

Fig. 1. Calculated impedance spectrum for a 1-D array with 50 μm kerf, 0.2 mm element size, and element height of 0.3 mm. The solid curve is for the case without element subdicing; the dashed curve is for the model with element subdicing.

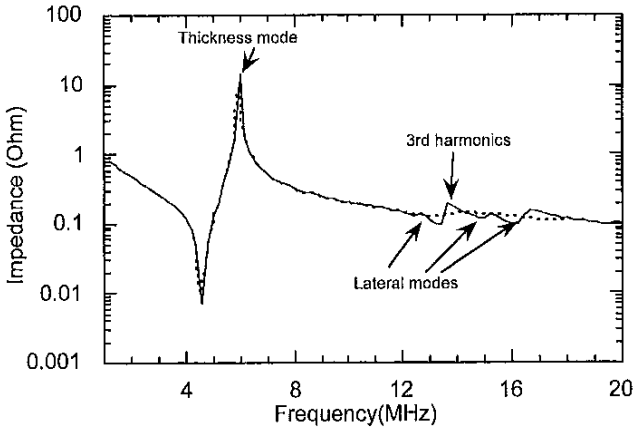

Fig. 2. The calculated impedance curve for a 5 MHz 1-D array transducer with 35 μm kerf width, 300 μm pitch, and 420 μm element height. For the solid curve, the Rayleigh damping ratios for the ceramic and the filler were set at $\beta_c = 3 \cdot 10^{-10}$ s and $\beta_p = 5 \cdot 10^{-10}$ s, respectively. For the dashed curve, the Rayleigh damping ratios for the ceramic and the filler were $\beta_c = 3 \cdot 10^{-10}$ s, and $\beta_p = 5 \cdot 10^{-9}$ s, respectively.

the comparison between the impedance spectra of two transducers with the same design but different kerf filler materials. The solid line is for a design using low loss filler material. Three lateral modes are visible in the impedance curve for this case. When the filler damping is increased by an order of magnitude in our simulation model, while keeping all other parameters unchanged, the lateral modes as well as the third harmonic disappeared (dashed line in Fig. 2).

The baffle effect for each element in an array was not given enough attention before. It is usually described by a cosine function assuming the baffle to be a pressure-release baffle and the array to be infinite in the elevation dimension. However, this assumption is not accurate for real transducers. Using numerical methods, we were able

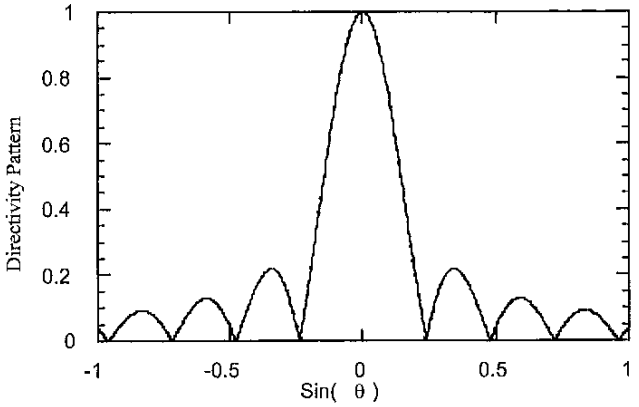

Fig. 3. The normalized directivity pattern of a uniformly vibrating square transducer in a rigid baffle. The transducer is a 5 mm × 5 mm square, and the center frequency is 1.25 MHz. The numerical results are identical with the analytic results.

to successfully calculate the baffle effect in realistic conditions. A direct computation of transducer beam pattern using the finite element method (FEM) was not successful because the water medium was too large and error accumulation rendered the solution unstable, particularly for the far field pressure distribution. To resolve this problem, we used a smaller FEM model to calculate the pressure and velocity distributions at the transducer surface, then used the BEM to solve the Helmholtz integral.

B. Verification of the Beam Pattern Obtained from Numerical Methods

We used two simple models to verify the numerical results. The first verification was a uniformly vibrating 5 mm by 5 mm square transducer with an infinite rigid baffle. The Helmholtz integral for the pressure distribution $p(x)$ is given by:

$$p(\mathbf{x}) = \int_S \left\{ p(\boldsymbol{\sigma}) \frac{\partial G(\mathbf{x}, \boldsymbol{\sigma})}{\partial n_\sigma} + i\omega\rho v(\boldsymbol{\sigma}) G(\mathbf{x}, \boldsymbol{\sigma}) \right\} ds(\boldsymbol{\sigma}) \tag{1}$$

where $G(\mathbf{x}, \boldsymbol{\sigma}) = \frac{1}{4\pi} \frac{e^{-ik|\mathbf{x}-\sigma|}}{|\mathbf{x}-\boldsymbol{\sigma}|}$ is the Green's function, σ is the space variable on the transducer surface, $p(\sigma)$ and $v(\sigma)$ are the pressure and velocity, respectively, at the transducer surface, and n_σ is the surface normal.

The first term in (1) is zero for a rigid baffle so that the integral can be simplified as:

$$p(\mathbf{x}) = \int_S \{ i\omega\rho v(\boldsymbol{\sigma}) G(\mathbf{x}, \boldsymbol{\sigma}) \} \, ds(\sigma) \tag{2}$$

One can solve (2) analytically, and the solution provides us a control check for the numerical results. The analytic and numerical results are identical as shown in Fig. 3, which confirmed the validity of our numerical procedure.

The second test is for a uniformly vibrating square piston transducer in a pressure-release baffle. For this model,

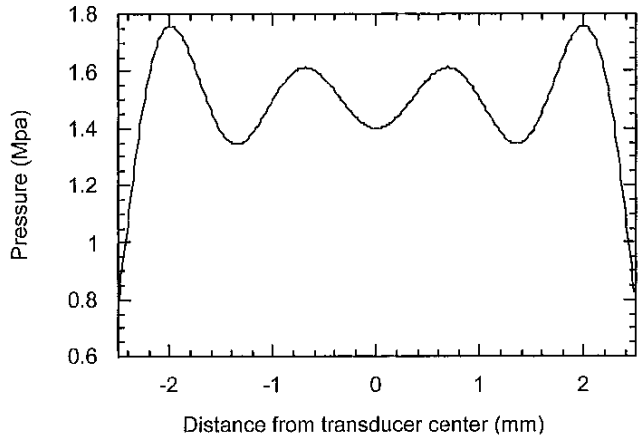

Fig. 4. The pressure amplitude distribution on the surface of a uniformly vibrating transducer immersed in water, the size of the square transducer is 5 mm × 5 mm with a center frequency of 1.25 MHz.

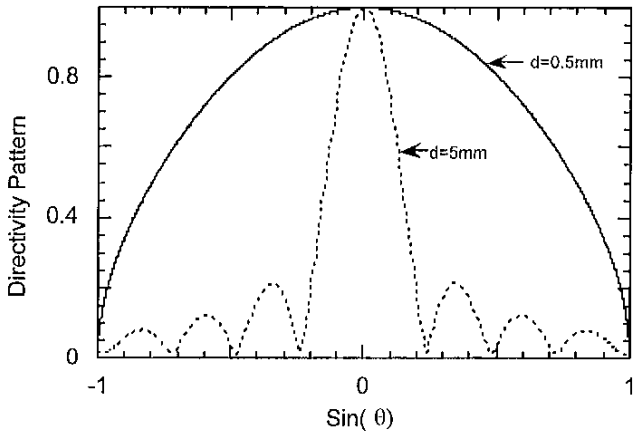

Fig. 5. Comparison between the normalized directivity patterns of two transducers with a diameter of 0.5 mm and 5 mm, respectively. The center frequency for both transducers is 1.25 MHz.

the second term $G(\mathbf{x}, \boldsymbol{\sigma})$ is zero; therefore, (1) can be rewritten as:

$$p(\mathbf{x}) = \int_S \left\{ p(\boldsymbol{\sigma}) \frac{\partial G(\mathbf{x}, \boldsymbol{\sigma})}{\partial n_\sigma} \right\} ds(\sigma) \tag{3}$$

In this model, the normal vibrating velocity is a constant, and the pressure distribution at the transducer surface may be calculated by using (3). The pressure distribution was nonuniform at the transducer surface, although the normal vibrating velocity is a constant (Fig. 4). The analytical solution of the directivity pattern is equal to the product of a *sinc* function and $\cos\theta$, in which the $\cos\theta$ term represents the effect of a pressure-release baffle [4]. The calculated directivity using (3) is exactly the same as the analytical solution as shown in Fig. 5 (the two curves overlap). The directivity pattern calculated in Fig. 5 is almost a half circle for a transducer of 0.5 mm square (solid curve), which is much smaller than the wavelength of 1.2 mm. The dashed line is for a 5 mm square, single-element transducer; and its dimension is much larger than the wavelength of 1.2 mm. Sidelobes appeared in the directivity pattern for the latter case.

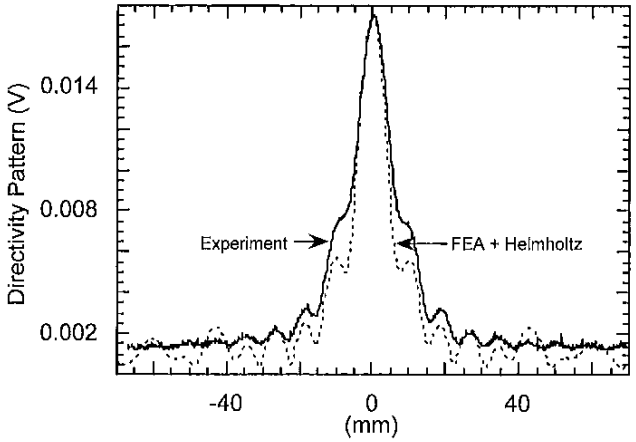

Fig. 6. The directivity pattern of a 32 element array transducer. The measurement was performed at a distance 30 cm from the face of the array; the peak value of the calculated pressure is normalized to the peak value of the measured voltage.

After the two confidence checks, our numerical code was applied to calculate the beam pattern of a 1-D array and compared to experimental measurements. Fig. 6 is the comparison of the calculated and measured directivity patterns for a 1-D array with all elements excited in phase (note: the calculated beam pattern was normalized to voltage based on the peak value of the experimental observations). The calculated results match reasonably well with the experimental results. Both the computations the experiments were performed using water as the medium.

C. Directivity Pattern of an Element Embedded in a 1-D Array

After the verification procedure described in the last section, the combined FEM and BEM method was applied to simulate the transducer beam pattern of one element embedded in a finite 1-D array. In this model, the baffle is neither a pressure-release type nor a rigid type; therefore, one cannot solve the problem analytically. Fig. 7 shows a 32-element 1-D array FEA model with partially diced backing, 2 matching layers, a fluid-structure interface layer, and a portion of the water medium. The kerf size is 0.1 mm, the element size is 0.15 mm, and the element height is 1.12 mm. Absorbing boundary conditions were applied at the boundaries of water medium to eliminate reflections.

As an example, we excited the 16th element in the array using a broadband pulse. The pressure and normal velocity distributions were obtained using harmonic analysis in the ANSYS® FEA code. Fig. 8 shows the real and imaginary parts of the pressure distributions, respectively, at the transducer surface. In the same computation, we also obtained the real and imaginary parts of the velocity distributions, respectively, at the surface of the array as shown

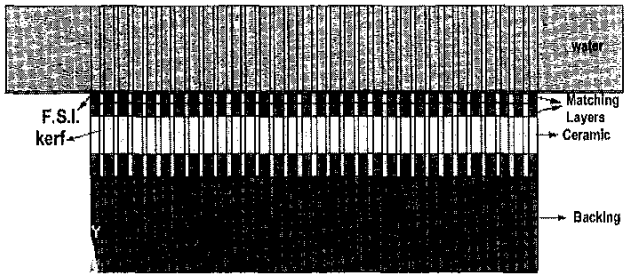

Fig. 7. The FEA model for a 32 element 1-D array. Both matching layer and part of backing were diced to reduce crosstalk.

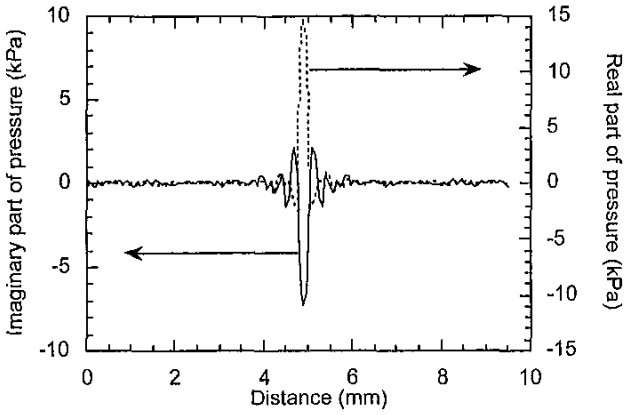

Fig. 8. The real (dashed line) and imaginary (solid line) parts of pressure distribution at the surface of a 32 element 1-D array when the 16th element was being excited.

in Fig. 9. Using these pressure and velocity distribution data, the directivity pattern of the 16th element can be calculated using the Helmholtz integral (1). The results are given in Fig. 10 as the solid line. For comparison, the analytic result of $sinc(2\pi\kappa d * \sin\theta) * \cos\theta$ is also shown in Fig. 10 by the dashed line. One can see that the directivity pattern obtained from FEA is much more complicated than the simple product of $sinc(2\pi\kappa d * \sin\theta) * \cos\theta$. There are many oscillations in the directivity pattern calculated by the FEA + BEM method. These variations are caused by the crosstalk among elements and reflect the effect of finite dimension with a nonuniform baffle.

The directivity pattern also depends on other factors, such as the properties of the kerf filler and the geometry of the array structure. Fig. 11 shows the comparison of the directivity patterns produced by arrays with a hard and a soft filler material, respectively. The intensity of the sound field is higher when the kerf is filled with harder material. For a soft kerf filler, the phase lagging between the kerf and the ceramic becomes larger, which causes the vibrating intensity of the whole array to decrease.

D. Beam Pattern of a 1-D Linear Array

Using the combined FEA+BEM method, we also calculated the beam pattern of the whole 1-D array transducer.

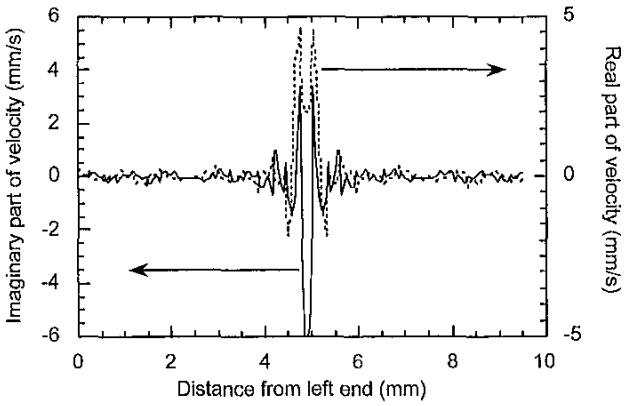

Fig. 9. The real (dashed line) and imaginary (solid line) parts of the velocity distribution on the surface of a 32 element 1-D array with the 16th element being excited.

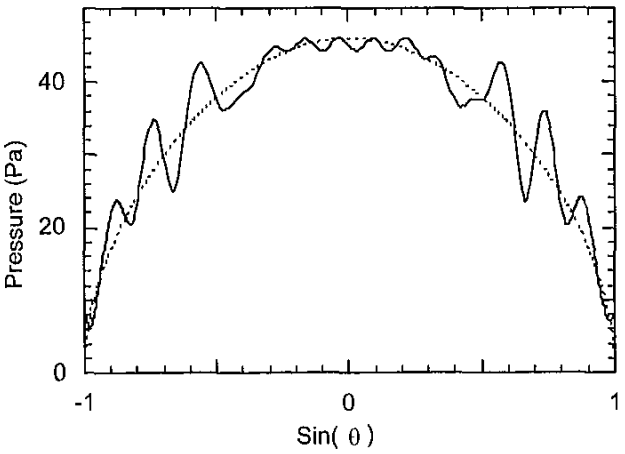

Fig. 10. The directivity pattern of one center element in a 1-D array.

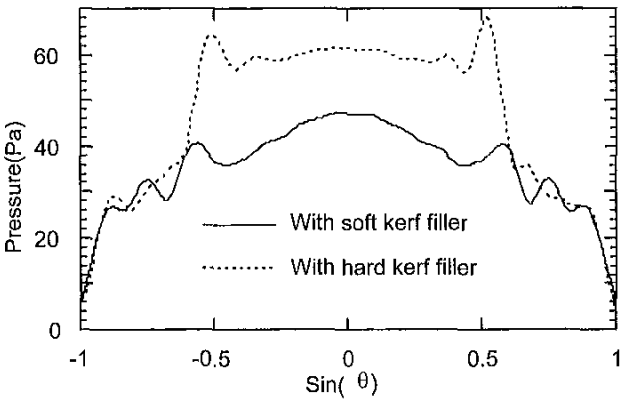

Fig. 11. Comparison between the directivity patterns (acceptance angle) of an array element with soft (solid line) and hard (dashed line) kerf filler.

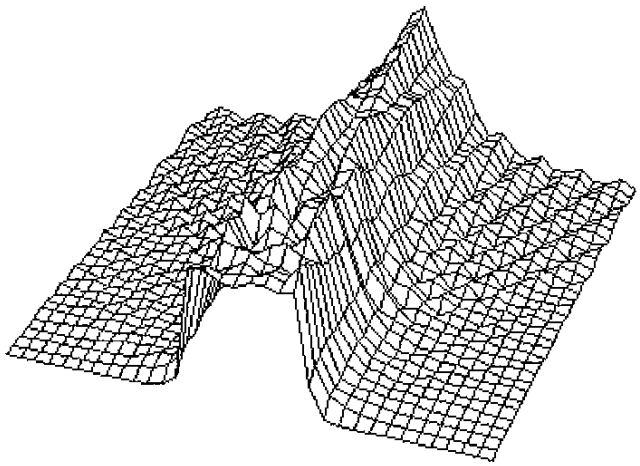

Fig. 12. The surface plot of the beam pattern of a 32 element 1-D linear array.

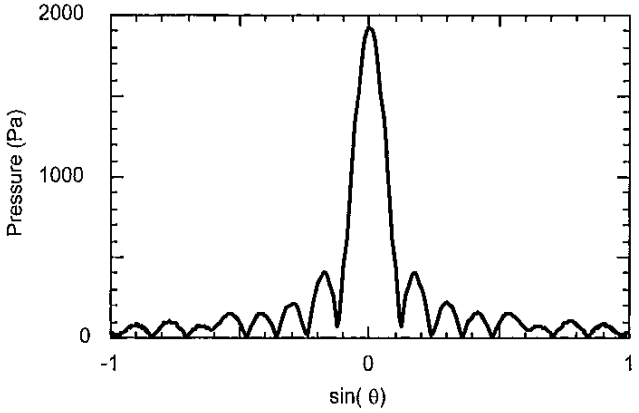

Fig. 13. The calculated directivity pattern of 32 elements in the center region of a 128 element linear array.

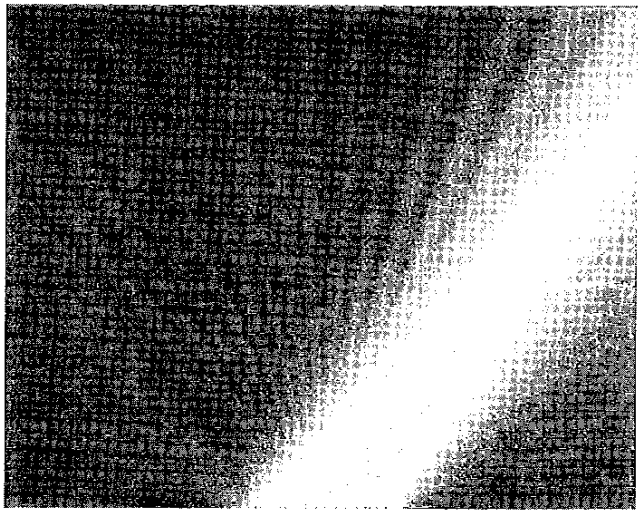

Fig. 14. Beam pattern of a phased array with 54° steering angle.

This FEA model array has a 0.6 mm pitch and 0.2 mm kerf, and the height of the element is 1 mm. The backing material is a composite of tungsten powder and polymer. The two quarter-wavelength matching layers were made of polymer and aluminum oxide powder; the aluminum oxide volume percentage was 17.5% for the inner matching layer and 7% for the outer matching layer. The kerf filler is a very light and soft polymer material. Except for the attenuation, all the input material parameters in the simulation model were measured experimentally.

Fig. 12 is a surface plot of the calculated beam pattern of this 1-D array. All detailed characteristics of the beam pattern, particularly the near-field variation, the focal point, beam size, and sidelobes are shown clearly in Fig. 12. The most significant result from the calculation is the detailed near-field beam pattern, which is very difficult to obtain experimentally because the measurement probe often interferes with the transducer beam to be measured. The calculations provided some critical information for transducer designs, such as beam width, focal distance, and sidelobe level (or grating lobe level). The directivity of partially excited array is plotted in Fig. 13. There are 128 elements in the FEA model array, but only 32 elements in the center region were excited for the directivity calculation. This partial excitation can help us to understand the baffle effect.

The establishment of the modeling procedure is very important for improving transducer designs and exploring new designs. Using the FEA simulation, we can optimize the element geometry, pitch size, and all the active and passive materials used in the transducer. In other words, it can help us find the best combination to produce a desired transducer.

The simulation procedure also can be used to study 1-D phased array by applying phase delayed electrical signals to consecutive elements. One can study the angular dependence of the beam pattern by steering the beam using simulation with phase-delayed excitation. Fig. 14 is a typical steered beam pattern with a steering angle of 54°. The width of the main beam, the sidelobe, and the focal distance all changed slightly as a function of the steering angle because the array has a finite size. The model phased array has a kerf size of 0.1 mm and a pitch size of 0.3 mm, which is equal to one-half of the wavelength, so there are no grating lobes [10]. The beam pattern in Fig. 14 was calculated by using harmonic analysis in ANSYS at 2.5 MHz, then use BEM to carry out the Helmholtz integral.

III. Crosstalk

The crosstalk in arrays degrades the contrast resolution and causes artifacts in ultrasonic imaging. It is of great importance to reduce the crosstalk level in designing better medical imaging transducers. Crosstalk has two sources: mechanical and electrical. Here we only analyze the mechanical crosstalk as the electrical crosstalk is less than −43 dB as analyzed in [4]. For convenience in the FEA, a

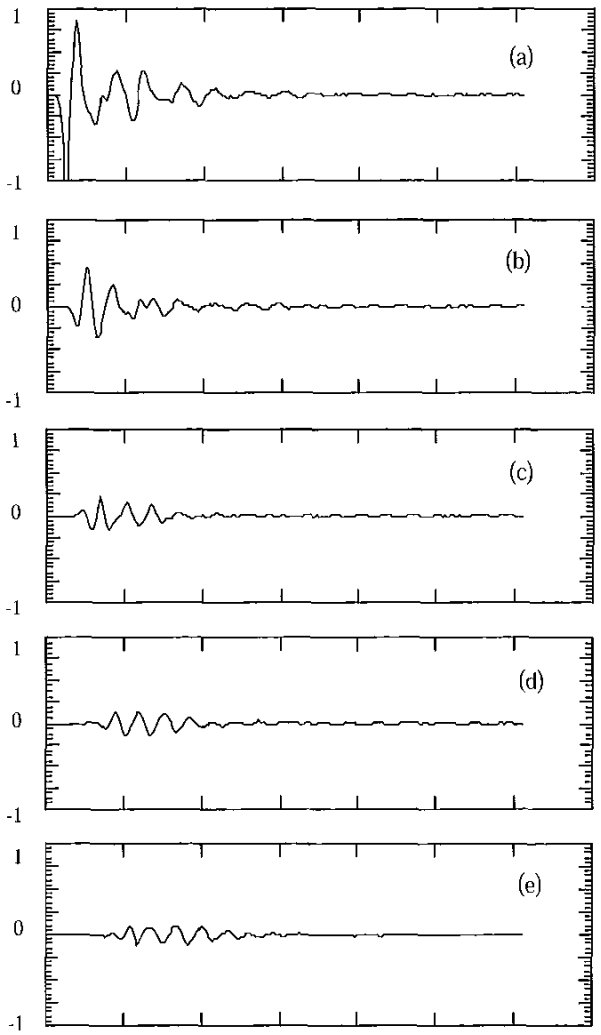

Fig. 15. Impulse responses of the excited element (a), first neighbor (b), second neighbor (c), third neighbor (d), and fourth neighbor (e), respectively.

new measure is defined for the mechanical crosstalk [5], [6] as the following:

$$\text{relative response} = -20\log\left(\frac{\text{RMS of the displacement of the excited element}}{\text{RMS of the displacement of the neighboring element}}\right).$$

Because we are using the RMS to define the mechanical crosstalk level, it has a unique value even for nonuniform displacement of each element. The new measure only reflects the strength of mechanical coupling; the electrical coupling was not included.

We have explored different kerf cutting schemes to reduce the mechanical crosstalk. The dimensions of the array under investigation are the same as that of the linear array shown in Fig. 7. The outer matching layer for this model design was a single sheet and the inner matching layer was diced together with the element. From Fig. 15(a) to (e), one can see that the amplitude of the impulse response of

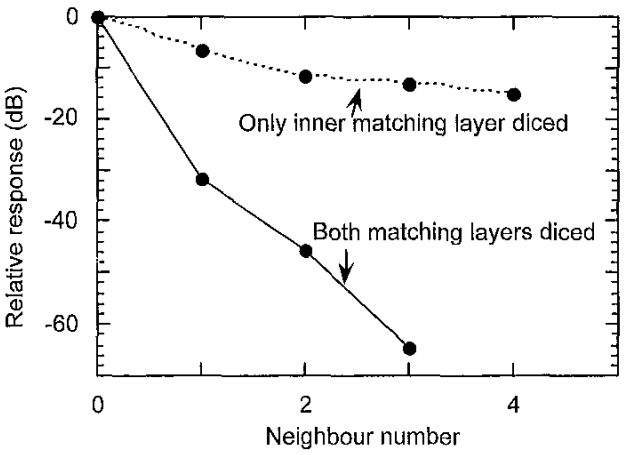

Fig. 16. Comparison of the crosstalk levels of array designs with one of the matching layers being diced and both matching layers being diced.

the neighboring elements gradually decreases with distance from the excited element. Our calculation showed that dicing both matching layers is very important for reducing the mechanical coupling between different elements (acoustic isolation). Fig. 16 plots the comparison of the mechanical crosstalk levels for two cases: 1) one inner matching layer was diced together with the element, and 2) both matching layers were diced together with the elements. As shown in Fig. 16 the crosstalk level is much reduced for the latter model. As a rule of thumb in transducer design, the crosstalk level for the nearest neighbor should be less than -30 dB in order to avoid artifacts in ultrasonic imaging; based on our calculations, the one layer dicing scheme is not sufficient to satisfy this requirement.

A lens is often used on top of the array transducer to change its focus. This lens may cause extra mechanical cross coupling if it is made of solid material. It was found that the main coupling mechanism is through shear wave; therefore, one way to reduce the lens coupling is to use materials that have very small shear modules. If the array is not air backed, the backing will also provide additional mechanical coupling. In practical designs, this problem is resolved by partially dicing the lossy transducer backing.

IV. Summary and Conclusions

We have reported a combined FEA and BEM study to simulate 1-D array transducers, which allowed us to study the subdicing effect, directivity pattern, baffle effect, and crosstalk in 1-D array transducers. It was shown that lateral modes might be decoupled from the thickness mode by either subdicing each element, which effectively moves the spurious modes to higher frequencies, or heavy damping. The baffle effects for an element embedded in a 1-D array have been accurately calculated using this combined simulation scheme. Three different types of baffles were studied, and the results were confirmed by both an-

alytical solutions and experiments. From the simulation results, the baffle effect cannot be simply represented by a $\cos\theta$ function as assumed in practice. Although harder filler materials in the kerfs can increase the sensitivity of the transducer, softer filler for the kerfs can reduce the mechanical coupling among elements and the strength of the lateral modes. The simulation results also indicated that the mechanical crosstalk level could be greatly reduced when both matching layers were diced. Lossy backing and lossy kerf filler also can help to broaden the acceptance angle response of each element in the array.

References

[1] K. Kirk Shung, M. B. Smith, and B. W. M. Tsui, in *Principles of Medical Imaging*. San Diego: Academic Press, 1992.

[2] G. S. Kino, in *Acoustic Waves*. New York: Prentice Hall, 1987.

[3] R. Lerch, H. Landes, and H. T. Kaarmann, "Finite element modeling of the pulse-echo behavior of ultrasound transducers," *Proc. IEEE Ultrason. Symp.*, 1994, pp. 1021 1026.

[4] R. Lerch, "Simulation of piezoelectric devices by two- and three-dimensional finite element methods," *IEEE Trans. Ultrason., Ferroelect., Freq. Contr.*, vol. 37, pp. 233–246, 1990.

[5] W. Qi and W. Cao, "Finite element analysis and experimental studies on the thickness resonance of piezocomposite transducers," *Ultrason. Imag.*, vol. 18, pp. 1–9, 1996.

[6] W. Qi and Wenwu Cao, "Finite element analysis of periodic and random 2-2 piezocomposite transducers with finite dimensions," *IEEE Trans. Ultrason., Ferroelect., Freq. Contr.*, vol. 44, pp. 1168–1171, 1997.

[7] W. Cao and W. Qi, "Plane wave propagation in finite 2-2 composite," *J. Appl. Phys.*, vol. 78, pp. 4627–4632, 1995.

[8] W. Cao and W. Qi, "Multisource excitations in a stratified biplane structure," *J. Appl. Phys.*, vol. 78, pp. 4640 4646, 1995.

[9] C. G. Oakley, "Analysis and development of piezoelectric composites for medical ultrasonic transducer applications," Ph.D. Dissertation, The Pennsylvania State University, University Park, PA, 1991.

[10] W. Friedrich, H. Kaarmann, and R. Lerch, "Finite element modeling of acoustic radiation from piezoelectric phased array antennas," *Proc. IEEE Ultrason. Symp.*, pp. 763 767, 1990.

Wenkang Qi received his B.S. and M.S. degrees in Biomedical Engineering in 1988 and 1991, respectively, from Tsinghua University, China. In 1997, he earned his Ph.D. degree in Bioengineering from The Pennsylvania State University. He joined GE Diasonics as an ultrasonic transducer researcher and designer in 1997.

Dr. Qi is a senior member of the IEEE and a member of the SPIE. His research interest is in the design of medical ultrasonic transducer arrays, ultrasound imaging systems, and other biomedical instruments.

Wenwu Cao received his B.S. degree in physics from Jilin University, Changchun, China, in 1982 and the Ph.D. degree in condensed matter physics from The Pennsylvania State University in 1987.

He is currently holding a joint appointment between the Department of Mathematics and the Materials Research Laboratory of The Pennsylvania State University as Associate Professor of Mathematics and Materials Science. He has conducted both theoretical and experimental research in the area of condensed matter physics and materials, including theories on proper- and improper-ferroelastic phase transitions and static and dynamic properties of domains and domain walls in ferroelectric and ferroelastic materials. He has also performed measurements on second- and third-order elastic constants, linear and nonlinear dielectric constants, and piezoelectric constants in single crytals and ceramics. His current interests also include the static and dynamic behavior of piezoelectric ceramic-polymer composites, simulation design of piezoelectric sensors, transducers and actuators for underwater acoustics, and medical ultrasonic imaging as well as ultrasonic NDE and signal processing.

Dr. Cao is a member of the Society for Industrial and Applied Mathematics and the American Physical Society.